J. Fluid Mech. (2004), *vol.* 501, *pp.* 213–229.
DOI: 10.1017/S002211200300747X Printed in the United Kingdom

Intermittency, pressure and acceleration statistics from hot-wire measurements in wind-tunnel turbulence

By A. GYLFASON, S. AYYALASOMAYAJULA AND Z. WARHAFT

Sibley School of Mechanical and Aerospace Engineering, Cornell University, Ithaca, NY 14853, USA

(Received 10 April 2003 and in revised form 15 October 2003)

From hot-wire anemometer measurements in active-grid wind-tunnel turbulence we have determined the Reynolds number dependence of the velocity derivative moments, the mean-squared pressure gradient, χ, and the normalized acceleration variance, a_0, over the Reynolds number range $100 \leqslant R_\lambda \leqslant 900$. The values of χ and a_0 were obtained from the fourth-order velocity structure functions. The derivative moments show power-law dependence on Reynolds number and the exponent is the same with or without shear. In particular, we find the derivative kurtosis, $K_{\partial u/\partial x} \sim R_\lambda^{0.39}$, and there is no evidence of the transition that has been observed in this quantity in some recent work. We find that at high Reynolds numbers, χ and a_0 tend to values similar to those obtained by direct particle tracking measurements and by direct numerical simulation. However, at lower Reynolds number our estimates of χ and a_0 appear to be affected by the evaluation technique which imposes strict requirements on local homogeneity and isotropy.

1. Introduction

Describing and explaining the intermittent nature of the small-scale velocity structure in fully developed turbulent flow continues to pose profound problems for the experimentalist and theoretician. First observed in velocity traces in the 1940s (Batchelor & Townsend 1949) and despite over a half century of concentrated effort (see reviews by Frisch 1995 and by Sreenivasan & Antonia 1997), there is still no broadly accepted theory or model to describe this phenomenon. Indeed it is still unclear how universal intermittency is (in the sense of its independence of large-scale boundary conditions), and whether it is due to the cascade process in which disturbances at the large scale are amplified with increasing wavenumber (e.g. Frisch 1995), or whether it is due to a more direct coupling between the large and small scales (e.g. Tsinober 2001). A generally accepted way of describing intermittency is by means of the kurtosis of the longitudinal velocity derivative, $K_{\partial u/\partial x} \equiv \langle(\partial u/\partial x)^4\rangle/\langle(\partial u/\partial x)^2\rangle^2$. Batchelor & Townsend (1949) observed values greater than 3 (the value of the kurtosis for a Gaussian distribution) and a number of experiments have shown (figure 6 of Sreenivasan & Antonia 1997) that $K_{\partial u/\partial x}$ increases with Reynolds number $R_\lambda \equiv \langle u^2\rangle^{1/2}\lambda/\nu$, where u is the longitudinal velocity component fluctuation, λ is the Taylor microscale $= [U^2\langle u^2\rangle/\langle(\partial u/\partial t)^2\rangle]^{1/2}$ (where U is the mean velocity) and ν is the kinematic viscosity. Typical traces of $u(t)$ and $\partial u/\partial t$ may be found in figure 2 of Warhaft (2000), from which the intermittent nature of the velocity is clearly evident.

Kolmogorov (1941, referred to herein as K41) phenomenology requires that $K_{\partial u/\partial x}$ be constant, independent of Reynolds number since K41 postulates that derivative statistics scale with ν and $\langle\varepsilon\rangle$ (the average rate of dissipation of the turbulence kinetic energy) only. The observation that $K_{\partial u/\partial x}$ depends on R_λ implies that the large-scale fluctuations play a role in determining the intermittency because R_λ is proportional to the velocity r.m.s. This in turn suggests a dependence on the way the flow is forced. Instead, statistical compilations of measurements in various geometries (figure 6 of Sreenivasan & Antonia 1997), indicate a power-law increase, $K_{\partial u/\partial x} \sim R_\lambda^n$, where $n \sim 0.35$, irrespective of the flow. The apparent lack of dependence on the nature of the large scales is consistent with the K41 postulate of local isotropy (PLI). According to PLI, at high Reynolds numbers, as the cascade proceeds from large to small scales, information on how the flow is forced at the large scales is lost. The observation that $K_{\partial u/\partial x}$ increases with Reynolds number is attributed to the increase in the level of intermittency (an aspect not taken into account in K41), and is not necessarily in conflict with PLI, although recent work (e.g. Pumir & Shraiman 1995; Shen & Warhaft 2000) suggests that intermittency and anisotropy may be related phenomena. The observed power-law increase is also consistent with phenomenological intermittency models (e.g. Meneveau & Sreenivasan 1991). For example the log–normal model for energy dissipation predicts $K_{\partial u/\partial x} \sim R_\lambda^{3\mu_2/2}$, where μ_2 is the intermittency parameter (Frisch 1995). Its value (Sreenivasan & Antonia 1997) is around 0.25, yielding $K_{\partial u/\partial x} \sim R_\lambda^{0.38}$.

Tabeling & Willaime (2002) (see also Tabeling *et al.* 1996) have challenged the observed power-law increase in $K_{\partial u/\partial x}$ by suggesting that subtle variations have been masked by the coarse variation in Reynolds number in the experiments. Their detailed measurements in a complex low-temperature helium gas flow produced by counter-rotating disks shows a transition at around $R_\lambda \sim 700$ (figure 3, Tabeling & Willaime 2002 and figure 4 below). They postulate that the transition is due to worm vortex breakdown, and suggest that it may be a universal characteristic of turbulence. If this is indeed the case, their suggestion poses a profound challenge to turbulence theory. One of the objectives of this paper is to examine the evolution of $K_{\partial u/\partial x}$ with Reynolds number by measuring $K_{\partial u/\partial x}$ over small increments of R_λ in simple wind-tunnel turbulence.

A related objective is to determine mean-squared pressure gradient and acceleration variance from the hot-wire measurements. Like the velocity derivative, these quantities are strongly affected by turbulence intermittency, exhibiting stretched exponential tails in their probability density functions (Voth, Satyanarayan & Bodenschatz 1998; Voth *et al.* 2002). As the Reynolds number increases the intermittency effects become more and more pronounced. Practical applications (e.g. Shaw 2003) require knowledge on how the acceleration variance and mean-squared pressure gradient vary with Reynolds number. Phenomenological models predict (as for the kurtosis) a power-law increase with R_λ (Voth *et al.* 2002; Hill 2002*a*). For example, assuming a log–normal model for the energy dissipation rate, it can be shown that the normalized acceleration variance $a_0 \equiv (1/3)\langle a_i a_i\rangle/\nu^{-1/2}\langle\varepsilon\rangle^{3/2} \sim R_\lambda^{9\mu_2/16}$ (Voth *et al.* 2002). For $\mu_2 = 0.25$ this yields $a_0 \sim R_\lambda^{0.14}$. In contrast K41 scaling (no intermittency) predicts a_0 is a constant, independent of Reynolds number.

Hill & Wilczak (1995, referred to herein as HW) and (Hill 2002*a*, *b*) have re-examined the earlier work of Heisenberg (1948), Obukhov (1949), Yaglom (1949), Obukhov & Yaglom (1951) and Batchelor (1951) in which pressure and acceleration statistics were related to the velocity fluctuations via the Navier–Stokes equations. HW provide relations that do not rely on the joint Gaussian assumption used in the

earlier work, a poor assumption in the light of the strong departures from Gaussian statistics at the small scales. (HW demonstrate, see also the results below, that the statistics of the small scales are those most relevant to the determination of the pressure and acceleration variances.) HW assume local isotropy, local homogeneity and incompressibility only. Their work provides the possibility of comparing direct numerical simulations (DNS) (Vedula & Yeung 1999; Gotoh & Fukayama 2001) and direct Lagrangian particle tracer experiments (Voth *et al.* 1998, 2002) with the Eulerian measurements taken in wind tunnels. As with the Kurtosis measurements of Tabeling & Willaime (2002), there is conflicting evidence in this area as well. The particle tracking measurements of Voth *et al.* (2002) show a complex dependence between the acceleration variance and R_λ, with a_0 first increasing and then levelling off at $R_\lambda \sim 700$, a result that appears to be in conflict with simple scaling arguments, with DNS (Vedula & Yeung 1999), and with HW. A possible connection between the Voth *et al.* (2002) results and the intermittency results of Tabeling & Willaime (2002) has been noted by Hill (2002*a*).

The HW theory relates the mean-squared pressure gradient, $\chi \equiv (1/\rho^2)\langle(\partial p/\partial x_i)(\partial p/\partial x_i)\rangle$, where ρ is the fluid density and p is the pressure fluctuation, to the velocity structure functions by

$$\chi = 4\int_0^\infty r^{-3}[D_{uuuu}(r) + D_{vvvv}(r) - 6D_{uuvv}(r)]\,\mathrm{d}r \tag{1}$$

where $D_{uuuu}(r)$ is the fourth-order structure function of the longitudinal velocity fluctuation u, $D_{vvvv}(r)$ is the fourth-order structure function of the transverse velocity component orthogonal to u, in this paper denoted as v, and $D_{uuvv}(r)$ is the mixed fourth-order structure function. The flow to be considered is decaying, active-grid turbulence, supplemented with some data in which there is shear in the direction transverse to the mean flow. Taylor's hypothesis is used to convert time series into spatial (downstream x-direction) series. Thus $\partial u/\partial x = -U^{-1}(\partial u/\partial t)$, etc.

Although the measurement of these fourth-order structure functions by means of an X-wire configuration appears to be straightforward, there are severe resolution problems. These will be discussed in detail. HW suggests that some of these difficulties may be alleviated if only a single wire can be employed for the measurement of χ. They suggest that

$$H_\chi \equiv 1 + \frac{\displaystyle\int_0^\infty r^{-3}[D_{vvvv}(r) - 6D_{uuvv}(r)]\,\mathrm{d}r}{\displaystyle\int_0^\infty r^{-3}D_{uuuu}(r)\,\mathrm{d}r} \tag{2}$$

may be constant for R_λ greater than a few hundred. Vedula & Yeung (1999) determined H_χ from DNS and showed that its value approaches a constant value of approximately 0.65 for R_λ greater than about 200. The utility of a constant value of H_χ is re-emphasized by Hill (2002*b*). From (2) it follows that

$$\chi = 4H_\chi \int_0^\infty r^{-3}D_{uuuu}(r)\,\mathrm{d}r. \tag{3}$$

Thus according to (3) only a single hot-wire anemometry probe (that measures the u component) is necessary to determine χ. Hill (2002*a*) also shows, again assuming local homogeneity, local isotropy and incompressibility, that the acceleration variance

is

$$\langle a_i a_i \rangle = \chi - \frac{35}{2}\nu\left\langle \left(\frac{\partial u}{\partial x}\right)^3 \right\rangle. \tag{4}$$

Hence $\langle a_i a_i \rangle$ can in principle be determined by an X-wire anemometer array, and if H_χ is constant, by a single component probe. Previous attempts to determine mean-squared pressure gradient and acceleration variance using hot-wire anemometry have been made by Pearson & Antonia (2001) and by Hill & Thoroddsen (1997).

This paper, then, has two objectives: first to determine $K_{\partial u/\partial x}$ in simple wind-tunnel flows and second to deduce from the Eulerian measurements of velocity in these flows, the mean-square pressure gradient and the acceleration variance.

2. Apparatus

As in our previous work, the experiments were performed in our two low-background-turbulence, open-circuit wind tunnels. The smaller tunnel (ST) is $40.7 \times 40.7\,\mathrm{cm}^2$ in cross-section and 4.5 m long (Sirivat & Warhaft 1983). Using the active grid (Mydlarski & Warhaft 1996, 1998) we could achieve a maximum value of R_λ of around 400. The larger tunnel (LT) is $91.4 \times 91.4\,\mathrm{cm}^2$ in cross-section and 9.1 m long (Yoon & Warhaft 1990). Here, with the active grid the maximum value of R_λ was around 750. Although we can obtain higher Reynolds numbers, the value of the dissipation scale $\eta \equiv (\nu^3/\langle\epsilon\rangle)^{1/4}$ becomes too small to properly resolve the velocity derivative, see below. To achieve higher values of R_λ with concomitantly larger values of η we used a shear generator and flow straighteners (Shen & Warhaft 2000). The effect of the anisotropy produced with the shear generator is discussed below.

Both wind tunnels are geometrically similar. The active grid in LT is almost identical to that used in ST; but in LT the mesh spacing M is 11.4 cm, which is two and a quarter times that in the ST. The LT grid has seven grid bars in the vertical direction and eight in the horizontal (the outermost horizontal grid bars were $(1/2)M$ from the tunnel walls). The grid in the ST has seven grid bars in each direction, with the outermost bars in both directions $1M$ from the walls (Mydlarski & Warhaft 1996, 1998). Thus, although the tunnel cross-sections are both $8M \times 8M$ there is a slight difference between the geometries of the two grids.

Experiments were performed with the active grid operating in either the synchronous or the random modes (Mydlarski & Warhaft 1996). In the synchronous mode the grid operation is parameterized by the Strouhal number $St \equiv 2\pi f M/U$ where f is the rotation rate of the bars. For the random mode, there is an added parameter, f_r, which is the frequency at which the direction of rotation is alloted by an equal-probability binary random variable generator (Mydlarski & Warhaft 1996). f was varied from 0.5 to 2.0 r.p.s. and there was no observed sensitivity of the results to its variation. Hence St does not play a role in dynamic similarity. For the random mode f_r/f was varied from 10 to 40 with f fixed at 1 r.p.s. There was a weak dependence on f_r/f, for the pressure and acceleration statistics, but the values of the normalized derivative statistics were independent of this ratio. Because higher values of R_λ can be achieved in the random mode, we will confine our results to this case. For the experiments reported here f and f_r/f were 1 r.p.s. and 20 respectively.

For dynamic similarity the mesh Reynolds number, $R_M \equiv UM/\nu$, f_r/f, and x/M (where x is the downstream distance from the grid) must be the same for the two

	Small tunnel No shear		Large tunnel No shear		Large tunnel With shear	
	Min R_λ	*Max* R_λ	*Min* R_λ	*Max* R_λ	*Min* R_λ	*Max* R_λ
R_λ	149	396	428	729	452	877
$U(\mathrm{m\,s^{-1}})$	2.98	7.26	3.94	7.80	3.72	8.94
$\langle u^2\rangle^{1/2}/U(\%)$	6.71	14.5	15.2	18.1	12.1	13.9
$\langle u^2\rangle/\langle v^2\rangle$	1.36	1.65	1.19	1.35	2.10	2.32
ℓ(m)	0.109	0.149	0.306	0.377	0.456	0.617
λ(mm)	10.9	5.65	10.7	7.76	15.1	10.6
η(mm)	0.456	0.144	0.263	0.146	0.361	0.181
$\langle\epsilon\rangle(\mathrm{m^2\,s^{-3}})$	0.07891	7.78	0.704	7.43	0.198	3.13
$-S_{\partial u/\partial x}$	0.505	0.538	0.562	0.575	0.546	0.586
$F_{\partial u/\partial x}$	6.17	9.16	9.58	11.4	9.94	13.1
ℓ_w/η	0.557	1.76	0.965	1.74	0.703	1.40

TABLE 1. Various flow parameters for the two tunnels used in the experiments to determine the logitudinal velocity derivative moments. $\langle\epsilon\rangle$ was determined from the expression $15(\nu/U^2)\langle(\partial u/\partial t)^2\rangle$. $\ell \equiv \langle u^2\rangle^{3/2}/\langle\epsilon\rangle$. *Min* R_λ and *Max* R_λ are the minimum and maximum values of R_λ for the various flows. For the shear experiment, the mean shear was approximately same as in the Shen & Warhaft (2000), i.e. $\partial U/\partial y \sim 10\,\mathrm{s^{-1}}$.

tunnels operating in the random mode. Our results show that when they were the same, the results of all statistics were identical.

The measurements were made using a single component probe for streamwise derivatives and with an X-array to measure the u and v components simultaneously for the acceleration and pressure variance measurements. Two different wire diameters were used: 1.27 μm (platinum–rhodium) and 3.05 μm (tungsten). The ratio of the sensing element hot-wire length, ℓ_w, to its diameter, d, was 200 in both cases. For the derivative measurements it is necessary to resolve to the order of a Kolmogorov length scale, η, and the finest wire (1.27 μm) must be used (see below). Our initial attempts to determine a_0 and χ with an X-wire array using the smaller wire resulted in inconsistencies because of difficulties in producing perfectly straight wires. Their geometry changed with heating and aging, resulting in measurements that were not reproducible from one day to the next. Thus for these measurements we used the 3.05 μm wires. The integrands (equation (1)) peak at around 5η–6η and we determined that the 3.05 μm wire was adequate to resolve these statistics. The spacing between the two wires in the X-array was 1 mm.

Table 1 lists the flow parameters including the ratio ℓ_w/η for the minimum and maximum R_λ of each particular flow studied for the determination of the derivative statistics. Table 2 lists the flow parameters for the study used to determine χ and a_0.

In all cases TSI probes were used and they were connected to Dantec 55M01 constant-temperature bridges. The wire over-heat ratio was 1.8. The signals were high-pass filtered to eliminate low-frequency, large-scale disturbances (typically less than 0.01 Hz) and low-pass filtered to remove high-frequency noise (varying from 2000 to 20 000 Hz depending on the value of R_λ). The data were digitized using a 16 bit A/D converter and typically 10^7 samples were taken for each data record. Further details of experimental procedure may be found in Shen & Warhaft (2000) and Mydlarski & Warhaft (1996, 1998).

	x/M	58.5		67.5	
		Min R_λ	*Max* R_λ	*Min* R_λ	*Max* R_λ
(*a*)	R_λ	189	404	168	369
	$U(\mathrm{m\,s^{-1}})$	2.84	7.62	2.83	8.19
	$\langle u^2\rangle^{1/2}/U(\%)$	8.60	10.8	7.91	10.2
	$\langle u^2\rangle/\langle v^2\rangle$	1.42	1.65	1.36	1.64
	ℓ(m)	0.147	0.198	0.126	0.187
	λ(mm)	11.6	7.34	11.2	7.08
	η(mm)	0.430	0.186	0.441	0.181
	$\langle\epsilon\rangle(\mathrm{m^2\,s^{-3}})$	0.099	2.84	0.089	3.17
	ℓ_w/η	1.42	3.29	1.38	3.38
(*b*)	R_λ	268	757	249	656
	$U(\mathrm{m\,s^{-1}})$	3.00	9.23	3.01	8.83
	$\langle u^2\rangle^{1/2}/U(\%)$	9.15	13.2	8.02	11.1
	$\langle u^2\rangle/\langle v^2\rangle$	1.15	1.32	1.15	1.31
	ℓ(m)	0.261	0.472	0.256	0.440
	λ(mm)	14.6	9.35	15.4	10.1
	η(mm)	0.455	0.173	0.498	0.200
	$\langle\epsilon\rangle(\mathrm{m^2\,s^{-3}})$	0.079	3.80	0.055	2.12
	ℓ_w/η	1.34	3.53	1.22	3.05

TABLE 2. Various flow parameters used in the experiments to determine H_χ: (*a*) ST (*b*) LT.

3. The measurement of kurtosis: sensitivity to probe resolution and turbulence intensity

Early in our investigation it became apparent that probe resolution played a vital role in the measurement of the kurtosis. To illustrate this we show measurements of $K_{\partial u/\partial x}$ performed in both tunnels (figure 1). In the ST, the Kolmogorov scale $\eta \equiv (\nu^3/\langle\epsilon\rangle)^{1/4}$ (where ν is the kinematic viscosity and $\langle\epsilon\rangle \equiv 15(\nu/U^2)\langle(\partial u/\partial t)^2\rangle$ is the average turbulence energy dissipation rate) is smaller than in the LT at the same Reynolds number (table 1).

It is evident (figure 1*a*) that $K_{\partial u/\partial x}$ begins to saturate due to resolution limitations at around $R_\lambda = 400$ in the ST and at about $R_\lambda = 700$ in the LT. At these values of R_λ, the ratio of wire length to Kolmogorov length, ℓ_w/η, was about 2. In the results section we will only report derivative data with $\ell_w/\eta \leqslant 1.75$. The values of ℓ_w/η as a function of R_λ are also shown in figure 1(*a*).

For the data obtained with the shear generator in place (Shen & Warhaft 2000) we achieved larger values of η at high R_λ than with the active grid alone. Thus we were able to extend our results to higher R_λ, while complying with the constraint that $\ell_w/\eta \leqslant 1.75$. These data extend the R_λ range to 900. We note (figure 1*b*) that the power law for the shear data has the same exponent, but a slightly higher prefactor than for the decaying turbulence. In figure 1(*b*) we have fitted the laws $K_{\partial u/\partial x} = 0.89R_\lambda^{0.39}$ for the decaying grid turbulence and $K_{\partial u/\partial x} = 0.94R_\lambda^{0.39}$ for the shear turbulence for the data of figure 1(*a*). The small difference in prefactor (0.89 vs. 0.94) may be reflecting the differences of the overall flows. If so, these results suggest that the dependence of $K_{\partial u/\partial x}$ on whether the shear is present or not is extremely weak. We note that the difference is approximately the same as our measurement error, i.e. 0.5 units in $K_{\partial u/\partial x}$.

By varying the downstream distance and the mean velocity we were able to vary the turbulence intensity at a particular R_λ to see how derivative statistics were affected. In

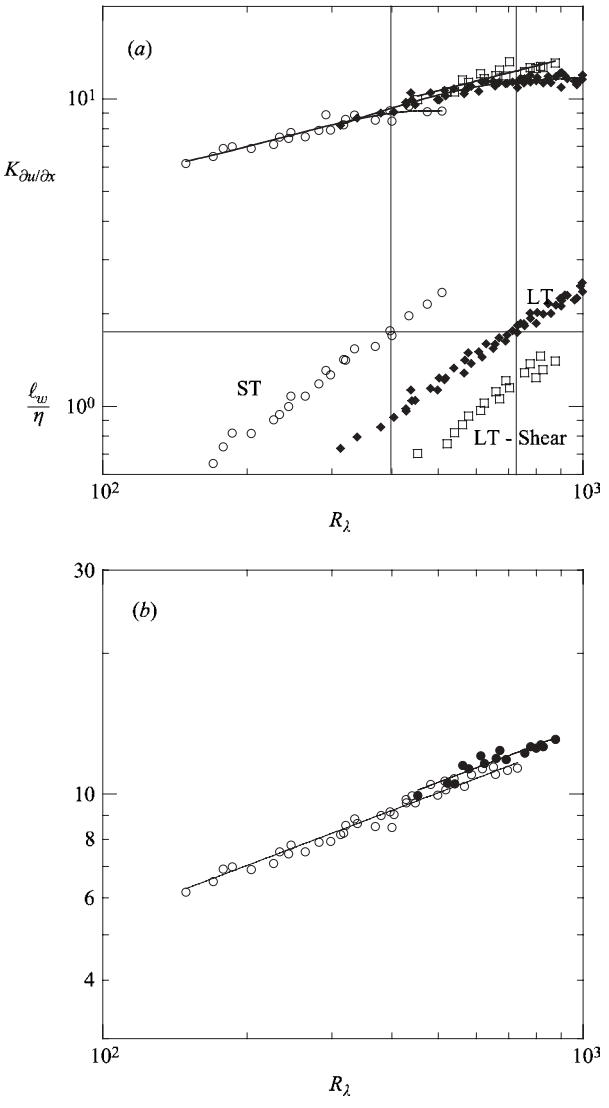

FIGURE 1. (*a*) The velocity derivative kurtosis, $K_{\partial u/\partial x}$, as a function R_λ for ST (open circles) and LT (solid diamonds, no shear and open squares, shear). The fit to the data is discussed in the text. Also shown is the ratio of the hot-wire length ℓ_w to the Kolmogorov length η (table 1). The horizontal line is at $\ell_w/\eta = 1.75$. (*b*) $K_{\partial u/\partial x}$ vs. R_λ for the data of (*a*) for which $\ell_w/\eta \leqslant 1.75$. Open circles, no shear, both tunnels. Solid circles, shear, LT. The fit to the data is $K_{\partial u/\partial x} = 0.89 R_\lambda^{0.39}$ (no shear) and $K_{\partial u/\partial x} = 0.94 R_\lambda^{0.39}$ (shear).

figure 2 we show $K_{\partial u/\partial x}$ and the derivative skewness $S_{\partial u/\partial x} \equiv \langle(\partial u/\partial x)^3\rangle / \langle(\partial u/\partial x)^2\rangle^{3/2}$ as a function of $\langle u^2\rangle^{1/2}/U$ at $R_\lambda \sim 500$. We see no systematic variation, at least up to a turbulence intensity of 20%.

4. Results

The Reynolds number dependence of the kurtosis

Figure 3 shows normalized third, fourth, fifth and sixth moments of the fluctuating derivative, $\partial u/\partial x$, as a function of R_λ. In all cases the distinction between the shear

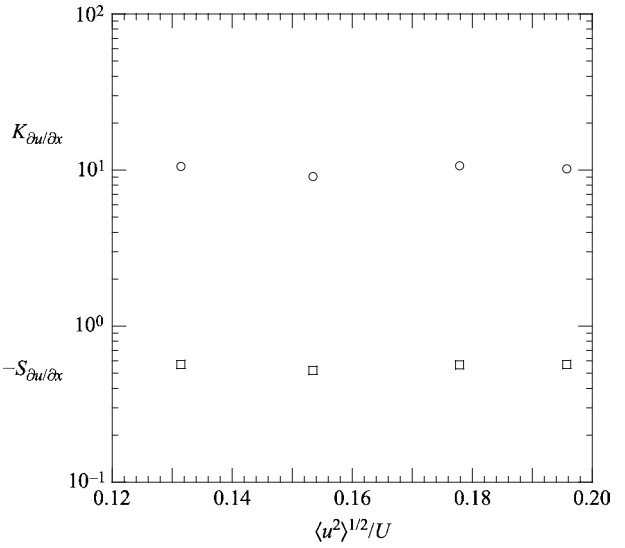

FIGURE 2. The derivative skewness (squares) and derivative kurtosis (circles) vs. the turbulence intensity. R_λ is approximately 500 for all cases, and the measurements were carried out in LT.

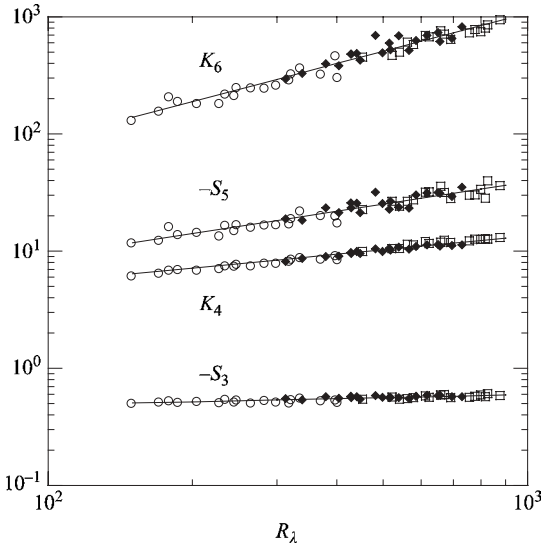

FIGURE 3. The normalized moments: $S_3 \equiv \langle(\partial u/\partial x)^3\rangle/\langle(\partial u/\partial x)^2\rangle^{3/2}$, $K_4 \equiv \langle(\partial u/\partial x)^4\rangle/\langle(\partial u/\partial x)^2\rangle^2$, $S_5 \equiv \langle(\partial u/\partial x)^5\rangle/\langle(\partial u/\partial x)^2\rangle^{5/2}$, and $K_6 \equiv \langle(\partial u/\partial x)^6\rangle/\langle(\partial u/\partial x)^2\rangle^3$. Symbols are the same as in figure 1(*a*). The fits to the curves are: $S_3 = 0.33R_\lambda^{0.09}$; $K_4 = 0.91R_\lambda^{0.39}$; $S_5 = 0.50R_\lambda^{0.63}$; and $K_6 = 0.62R_\lambda^{1.08}$. (The notation K_4 is used interchangeably with $K_{\partial u/\partial x}$ in this paper).

data and the decaying grid data is very small. The power laws that we fit to the data are $S_3 = -0.33R_\lambda^{0.09}$, $K_4 = 0.91R_\lambda^{0.39}$, $S_5 \equiv -\langle(\partial u/\partial x)^5\rangle/\langle(\partial u/\partial x)^2\rangle^{5/2} = 0.50R_\lambda^{0.63}$ and $K_6 \equiv \langle(\partial u/\partial x)^6\rangle/\langle(\partial u/\partial x)^2\rangle^3 = 0.62R_\lambda^{1.08}$. The exponents are very close to atmospheric measurements of Antonia, Chambers & Satyaprakash (1981). Their results extend to $R_\lambda \sim 10^4$ and they find $S_3 \sim -R_\lambda^{0.11}$, $K_4 \sim R_\lambda^{0.31}$, $S_5 \sim -R_\lambda^{0.61}$ and $K_6 \sim R_\lambda^{1.0}$. (Their data are more sparse than ours, and there is significantly more scatter.)

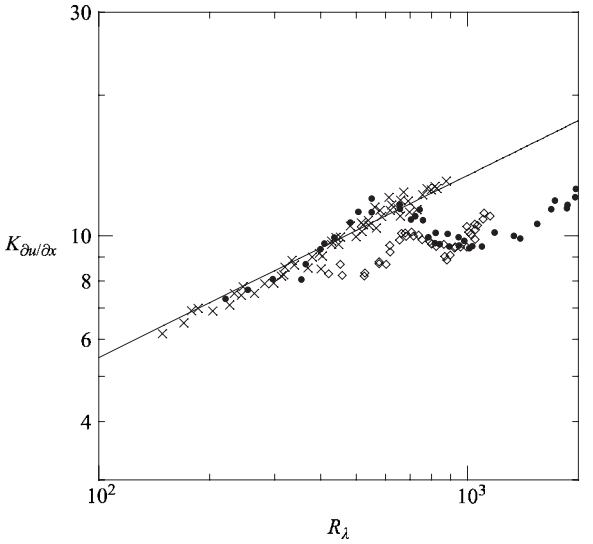

FIGURE 4. Comparison of the derivative kurtosis vs. R_λ for the present work (crosses), the Tabeling & Willaime (2002) experiment (solid circles) and the Pearson & Krogstad (2001) experiment (open diamonds). Here we do not discriminate between the ST and the LT (with or without shear), i.e. the crosses are the same set of data as in figure 3 (K_4).

As mentioned in the introduction, Tabeling & Willaime (2002 and references therein; see also Tabeling *et al.* 1996) have observed a transition at $R_\lambda \sim 700$ of the dependence of $K_{\partial u/\partial x}$ on R_λ. Data from figure 3 of their paper are replotted in figure 4, along with results of Pearson & Krogstad (2001). Notice that the Tabeling–Willaime data show a rise at $R_\lambda \sim 500$, followed by a pronounced dip at $R_\lambda \sim 700$ (this is more striking on their linear–linear plot). The Pearson & Krogstad data show an earlier transition, at $R_\lambda \sim 400$. Our data show no sign of a departure from a power-law dependence in the range $150 \leqslant R_\lambda \leqslant 900$. Note the extremely good agreement between Tabeling & Willaime's and our data for $R_\lambda \leqslant 400$.

The data of Pearson & Krogstad (2001) were obtained using conventional hot-wire anemometry and the probe resolution was good, with ℓ_w/η less than 2. Their flow, however, was complicated, with a checker-board grid arrangement (the so-called NORMAN grid, Pearson, Krogstad & van de Water 2000) in the centre of a large (2.7 m $\times$ 1.8 m cross-section) wind tunnel. The flow was undoubtedly strongly inhomogeneous at the large scales. Their observation of the non-monotone evolution of $K_{\partial u/\partial x}$ shows that under some circumstances, the small-scale statistics can be strongly affected by the large-scale boundary conditions. We will return to this in the discussion. Pearson & Krogstad (2001) attribute the bump they observe to the same 'mixing transition' suggested by Tabeling & Willaime (2002).

The Tabeling–Willaime experiments were conducted in a closed low-temperature helium gas flow. At each end of a cylindrical container the turbulence was generated by means of counter-rotating disks. The measurement points were spaced away from the centreline of the cylinder so there would be sufficient mean flow for the hot-wire anemometers to perform properly. (A mean convection velocity is required since hot wires operate in a forced convective mode). Undoubtedly the motion of large-scale flow was complicated. The measurements were made with a probe that was as wide as it was long. (In conventional hot-wire anemometry the probe sensing element is very

thin; the probe resolution being set by its overall length; see § 3 above). Although the experiments were very carefully carried out, and many of the effects of the probe such as the effects of vortex shedding, turbulence intensity (which was as large as 30% in some of their measurements) were examined, some issues remain. In particular the probe diameter was of order η (in conventional hot-wire experiments it is $\sim 0.005\eta$), and this could affect the nature of the probe interaction with the small eddies. While we do not know whether this or other factors did indeed complicate their results, because of the combination of the flow characterics and the probe, we believe that more work is required before their results can be accepted. In particular probe and flow effects need to be studied separately.

Whatever the case, it is quite apparent from figure 4 that neither the Tabeling & Willaime nor the Pearson & Krogstad results are universal.

Deduction of the acceleration variance and the mean-squared pressure gradient from the hot-wire measurements

As outlined in the introduction, HW have deduced expressions for the mean-squared pressure gradient, χ, and the acceleration variance, $\langle a_i a_i \rangle$, assuming local homogeneity and local isotropy. Unlike earlier work, the assumption of joint Gaussian probability distributions for velocity derivatives at two points, is not used. The expressions for χ and $\langle a_i a_i \rangle$ are given in (1) and (4), above.

There are serious difficulties in determining χ and $\langle a_i a_i \rangle$ from the HW expressions because of the difficulty of achieving precise local homogeneity and local isotropy in experiments. Although there is evidence that at high Reynolds numbers the transverse and longitudinal structure functions will achieve the same scaling exponents in the inertial range, a requirement for local isotropy for the second- and third-order structure functions, the Reynolds number at which this occurs appears to be extremely high. Thus in shear flows at $R_\lambda \sim 1000$ the scaling exponent of the v structure function is different to that of u at second (and higher) order (Warhaft & Shen 2002) and even at $R_\lambda \sim 10^4$ Dhruva, Tsuji & Sreenivasan (1997) find that the scaling exponent for the v structure function is slightly smaller than that of u structure function. Equality of the structure function scaling exponents is better in decaying, nearly locally isotropic, turbulence than in shear flow (Shen & Warhaft 2002). The effects of differences in scaling exponents in determining χ and $\langle a_i a_i \rangle$ are discussed by Nelkin & Chen (1998). Moreover HW (see also Nelkin & Chen 1998) showed that in the integral in (1) the second and third terms nearly cancel, giving rise to further difficulties in determining χ and $\langle a_i a_i \rangle$ (see figure 7 below).

Examples of the fourth-order structure functions of $D_{uuuu}(r/\eta)$, $D_{vvvv}(r/\eta)$ and $D_{uuvv}(r/\eta)$ are shown in figure 5, for the present no-shear (figure 5*a*) and shear experiment (figure 5*b*), carried out at almost the same Reynolds numbers ($R_\lambda = 421$ and 408 respectively). It is quite evident that for the case with shear, the v structure function is qualitatively different to that of the u structure function, the former having essentially no scaling range. Because of the pronounced effects of shear on the inertial range, in the following we will confine ourselves to the decaying grid turbulence data. Also shown in figures 5(*c*) and 5(*d*) are examples of the fourth-order structure functions at low and high Reynolds numbers (168 and 656 respectively) for the no-shear case. At the low R_λ the v structure function is qualitatively different to the u structure function and only at high R_λ do they tend to become similar. So, even for the no-shear case, we might expect that these differences will affect the estimate of the H_χ and a_0.

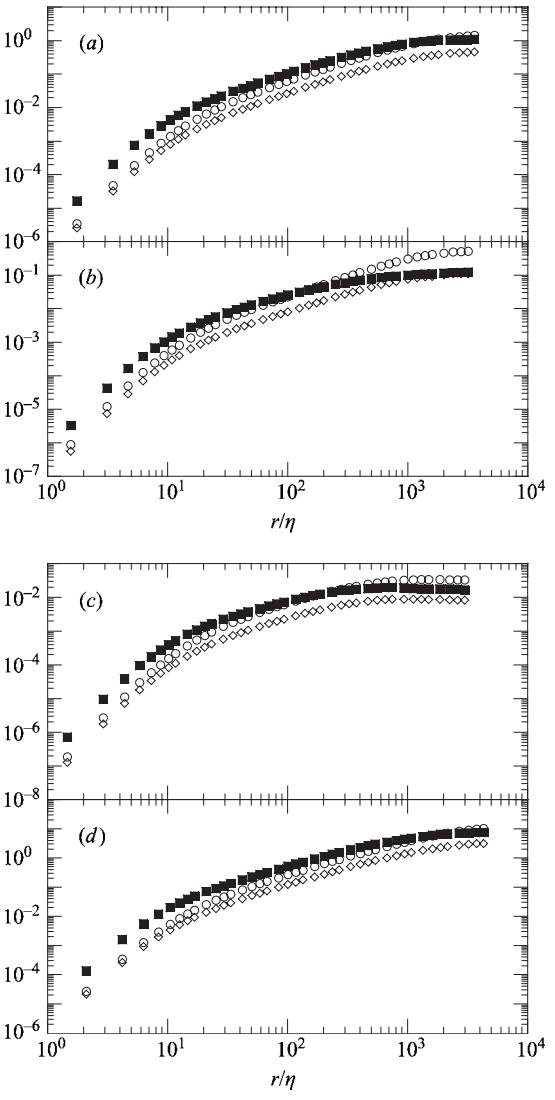

FIGURE 5. The fourth-order structure functions as a function of r/η. (*a*) LT, no shear, $R_\lambda = 421$; (*b*) LT, shear, $R_\lambda = 408$; (*c*) ST, no shear, $R_\lambda = 168$ and (*d*) LT, no shear, $R_\lambda = 656$. Open circles, the longitudinal structure function $D_{uuuu}(r/\eta)$; solid squares, the transverse structure function $D_{vvvv}(r/\eta)$; and the open diamonds, the mixed structure function $D_{uuvv}(r/\eta)$.

For the decaying turbulence experiments, figure 6 shows the structure function ratios D_{vv}/D_{uu}, D_{uuvv}/D_{uuuu} and D_{vvvv}/D_{uuuu}, all as functions of r/η, at two Reynolds numbers, $R_\lambda = 168$ and 656. The inertial-range plateau for both second- and fourth-order quantities only occurs at the higher Reynolds number. In the light of this it is instructive to see how χ, H_χ and a_0 determined from these fourth-order structure functions evolve with R_λ.

Figure 7 shows the total integrand of equation (1) as well as its components, $(r/\eta)^{-3} D_{uuuu}(r/\eta)$, $(r/\eta)^{-3} D_{vvvv}(r/\eta)$ and $6(r/\eta)^{-3} D_{uuvv}(r/\eta)$: in (*a*) and (*b*) we compare these functions at low and high Reynolds numbers, while in (*c*) and (*d*) we compare them at approximately the same R_λ, but from measurements done in the ST and

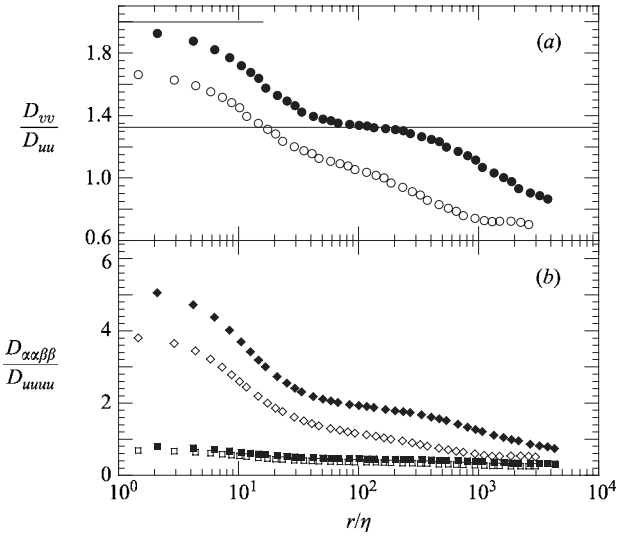

FIGURE 6. Ratios of structure functions. Filled symbols, LT, $R_\lambda = 656$; open symbols ST, $R_\lambda = 168$. (*a*) Circles, $D_{vv}(r/\eta)/D_{uu}(r/\eta)$; (*b*) diamonds, $D_{vvvv}(r/\eta)/D_{uuuu}(r/\eta)$ and squares, $D_{uuvv}(r/\eta)/D_{uuuu}(r/\eta)$. For (*a*) the isotropic ratios for the inertial and dissipation ranges are shown on the figure with straight lines.

LT. Note that the peak of these functions occurs at 5η–6η and the wire resolution is sufficient to resolve these scales. At smaller r/η we may have some resolution problems. Our measurements resolve to 2η–3η but tests in which we varied the shapes of the curves for $r/\eta \leqslant 3$ showed an insignificant effect on the integral. We note also that although $(r/\eta)^{-3}D_{vvvv}(r/\eta)$ and $6(r/\eta)r^{-3}D_{uuvv}(r/\eta)$ (equation (1)) are nearly equal in magnitude, their difference was found to vary systematically with Reynolds number. From this we were able to calculate the normalized pressure variance, $\chi/(\langle\varepsilon\rangle^{3/2}\nu^{-1/2})$ (equation (1)), H_χ (equation (2)) and $(1/3)\langle a_i a_i\rangle/(\langle\varepsilon\rangle^{3/2}\nu^{-1/2}) \equiv a_0$, the normalized acceleration variance (equation (4), with χ determined from equation (1)). These are shown in figures 8(*a*), 8(*b*) and 8(*c*).

All functions increase with Reynolds number. There is a very good overlap between the measurements done in the small and large tunnels, providing further support that resolution does not play a role. There appears to be a weak dependence on x/M suggesting that the method of evaluating these quantities may be sensitive to homogeneity and other evolving flow characteristics. As mentioned in § 2, there was also a weak dependence on the mode of operation of the active grid. This dependence (not shown here) was comparable to the dependence on x/M. Also shown in figure 8 are the direct numerical simulations of H_χ by Vedula & Yeung (1999) (figure 8*b*) and the acceleration variance measurements determined by particle tracking techniques (Voth *et al.* 2002) and the DNS of Vedula & Yeung (1999) (figure 8*c*). Hill (2002*a*) also presents computations by Gotoh (see Hill's figure 2) and shows they are consistent with the Vedula & Yeung (1999) DNS. We discuss the disparities in these results in the following section.

5. Discussion

We begin with the derivative statistics. The flows investigated here are attempts to create ideal decaying grid turbulence and ideal homogeneous shear. In the former the

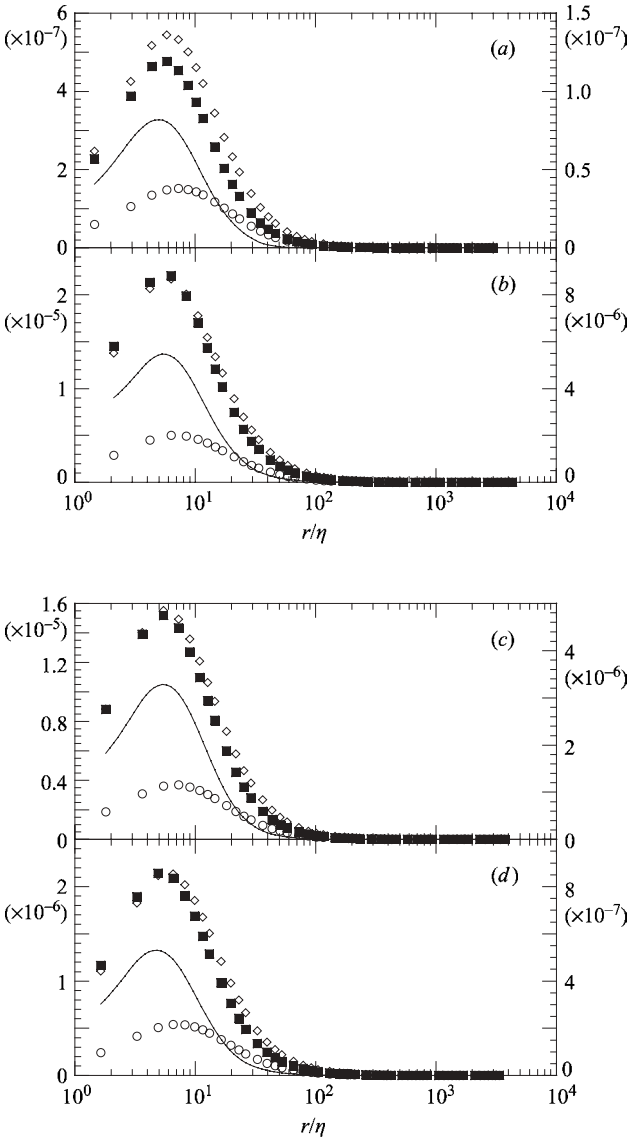

FIGURE 7. The integrands of equation (1) for (*a*) ST, $R_\lambda = 168$; (*b*) LT, $R_\lambda = 656$; (*c*) ST, $R_\lambda = 348$ and (*d*) LT, $R_\lambda = 360$. Left-hand axis, separate components of integrand: circles, $(r/\eta)^{-3} D_{uuuu}(r/\eta)$; squares, $(r/\eta)^{-3} D_{vvvv}(r/\eta)$; diamonds, $6(r/\eta)^{-3} D_{uuvv}(r/\eta)$. Right-hand axis, full integrand: solid line, $(r/\eta)^{-3}(D_{uuuu}(r/\eta) + D_{vvvv}(r/\eta) - 6D_{uuvv}(r/\eta))$.

objective is to realize isotropy at all scales; in the latter it is to realize homogeneity in the mean and higher-order moments. Those conditions can only be achieved in an approximate way in the laboratory. Nevertheless, departures from isotropy (in the decaying grid turbulence) and from homogeneity (in the homogeneous shear flow) are not pronounced (Mydlarski & Warhaft 1996; Shen & Warhaft 2000) and the result is that derivative statistics evolve in a straightforward power-law manner with Reynolds number (figure 3).

By contrast, the Tabeling & Willaime (2002) experiment and the Pearson & Krogstad (2001) experiment (figure 4) use flows that appear to be highly

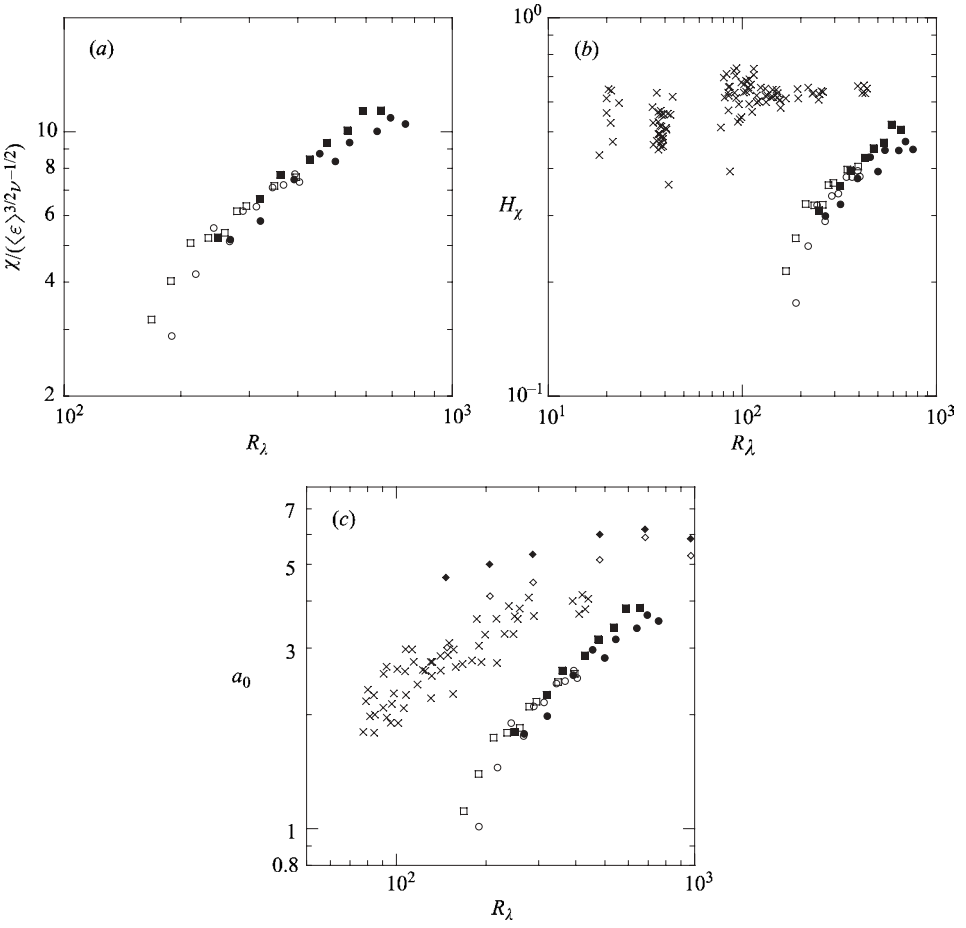

FIGURE 8. (*a*) The normalized mean-squared pressure gradient, $\chi/(\langle\varepsilon\rangle^{3/2}\nu^{-1/2})$, as a function of R_λ. (*b*) H_χ, (equation (2)) as a function of R_λ. Also shown are the DNS values (crosses) of Vedula & Yeung (1999), supplemented by some of their new computations at high R_λ ($R_\lambda \sim 400$, Vedula & Yeung, private communication). (*c*) The normalized acceleration variance, a_0, as a function of R_λ. The crosses are the data of Vedula & Yeung (1999) and the filled and open diamonds are particle tracking data of Voth *et al.* (2002) for the transverse and longitudinal directions respectively. Open symbols ST; filled symbols LT. Circles $x/M = 58.5$; squares $x/M = 67.5$.

inhomogeneous at the large scales. The level of large-scale inhomogeneity may be such that it is directly transmitted to the small scales. While this is in contradiction to the PLI and to the Kolmogorov cascade, it is not unreasonable to expect that if the large-scale inhomogeneity is sufficiently severe, a direct interaction would be possible. Thus we conjecture that the bumps observed in the experiments cited above are peculiar to the particular flows. It would be fruitful to study the effects on small scales by systematically varying the intensity of large-scale inhomogeneities. The results of figure 4 clearly indicate that small-scale statistics are flow-dependent quantities for complex flows. This is generally overlooked in turbulence modelling.

We now return to the disparities in the determination of H_χ, a_0 and χ by using the various experimental and computational techniques (figure 8*b*, *c*). It appears that a_0 and χ are less universal than derivative statistics, at least to $R_\lambda \sim 1000$. For example

there are no strong assumptions made in the estimates of Voth *et al.* (2002) or in Vedula & Yeung (1999), yet the values of a_0 are quite different, suggesting effects of boundary conditions at low and moderate Reynolds numbers. It is quite possible that above $R_\lambda \sim 1000$ the results of different experiments (and techniques) might converge. Indeed, there is a suggestion of this in figure 8(*c*). It needs to be emphasized that $R_\lambda = 1000$ is a very high value, and that the lack of universality up to that value may present problems for the modelling and design of fluid systems.

The present experimental data evolve with R_λ in quite a different manner to the Vedula & Yeung (1999) DNS (figure 8*b*) and the Voth *et al.* (2002) particle trajectory measurements (figure 8*c*) although at the highest Reynolds numbers the magnitudes of a_0 are reasonably consistent with the particle trajectory measurements and the DNS. The DNS are initialized to be isotropic, and therefore it may be expected that H_χ would reach its asymptotic value at a lower Reynolds number than in the experiment. On the other hand, we do not think that the particle trajectory experiments, done with rotating blades stirring the fluid from above and below (Voth *et al.* 2002), should attain local isotropy at lower Reynolds numbers than in grid turbulence. Indeed Voth *et al.* (2002) show that even at their highest $R_\lambda (\sim 1000)$ there is residual anisotropy, and for low R_λ it is pronounced. Thus we attribute the difference in the evolution of a_0 (figure 8*c*) between Voth *et al.* (2002) and the present experiment largely to the different ways in determining a_0: the Voth *et al.* measurements and analysis do not rely on the assumption of local isotropy and homogeneity, and therefore should be reliable at all Reynolds numbers. However, we might expect χ, H_χ and a_0 to be somewhat flow dependent, particularly at low R_λ, and therefore we could expect some differences between different flows. We note that it is not possible to extrapolate the subsequent evolution of a_0 from either the Voth *et al.* (2002) data or from the present set of measurements. Thus neither experiment can answer the question of whether a_0 remains constant or has a weak R_λ dependence at high R_λ. Experiments at much higher Reynolds number will be needed to address this issue.

6. Conclusions

In this work we have determined the mean-squared normalized pressure gradient, $\chi/(\langle\varepsilon\rangle^{3/2}\nu^{-1/2})$, the acceleration variance, a_0, and the parameter H_χ from Eulerian hot-wire measurements using the HW relations ((1) to (4) above). Although we have found that our estimates are affected by anisotropy and flow boundary conditions at low Reynolds numbers, at higher Reynolds numbers our values of a_0 and H_χ are in reasonable agreement with results from particle tracking experiments (Voth *et al.* 2002) and DNS (Vedula & Yeung 1999). Thus we find that H_χ has a value of approximately 0.5 at $R_\lambda = 800$ (figure 8*b*), while a_0 is approximately 4 at $R_\lambda = 800$ (figure 8*c*). Both still appear to be increasing with R_λ.

While the acceleration and pressure fluctuation statistics show Reynolds number dependences that are a function of flow anisotropy and boundary conditions when calculated using (1), the velocity derivative moments appear to be unaffected, showing a power-law evolution that is consistent with a wide variety of previous experiments (figure 3). A small exception to this occurs in the comparison of the no-shear and shear statistics (figure 1*b*). Here the prefactor of the power law is slightly higher for the shear than the no-shear case. Our results show no evidence of the 'bump' or transition in the derivative moments that has been observed in the experiments of Tabeling & Willaime (2002).

This work was supported by the US National Science Foundation. We thank Greg Voth, Eberhard Bodenschatz, Lance Collins, Stephen Pope and K. R. Sreenivasan for some discussions, and Reginald Hill for comments on an earlier draft of the manuscript.

REFERENCES

Antonia, R. A., Chambers, A. J. & Satyaprakash, B. R. 1981 Reynolds number dependence of high-order moments of the stream wise turbulent velocity derivative. *Boundary–Layer Met.* **21**, 159–171.

Batchelor, G. K. 1951 Pressure fluctuations in isotropic turbulence. *Proc. Camb. Phil. Soc.* **47**, 359–374.

Batchelor, G. K. & Townsend, A. A. 1949 The nature of turbulent motion at large wave-numbers. *Proc. R. Soc. Lond.* A **199**, 238–255.

Dhruva, B., Tsuji, Y. & Sreenivasan, K. R. 1997 Transverse structure functions in high-Reynolds number turbulence. *Phys. Rev.* E **56**, R4928–R4930.

Frisch, U. 1995 *Turbulence: The Legacy of A.N. Kolmogorov*. Cambridge University Press.

Gotoh, T. & Fukayama, D. 2001 Pressure spectrum in homogeneous turbulence. *Phys. Rev. Lett.* **86**, 3775–3778.

Heisenberg, W. 1948 Zur statistichen theorie der turbulenz. *Z. Physik* **124**, 628–657.

Hill, R. J. 2002*a* Scaling of acceleration in locally isotropic turbulence. *J. Fluid Mech.* **452**, 361–370.

Hill, R. J. 2002*b* Possible alternative to R_λ-scaling of small-scale turbulence statistics. *J. Fluid Mech.* **463**, 403–412.

Hill, R. J. & Thoroddsen, S. T. 1997 Experimental evaluation of acceleration correlations for locally isotropic turbulence. *Phys. Rev.* E **55**, 1600–1606.

Hill, R. J. & Wilczak, J. 1995 Pressure structure functions and spectra for locally isotropic turbulence. *J. Fluid Mech.* **296**, 247–269 (referred to herein as HW).

Kolmogorov, A. N. 1941 The local structure of turbulence in incompressible viscous fluid for very large Reynolds numbers. *Dokl. Akad. Nauk SSSR* **30**, 299–303 (referred to herein as K41).

Meneveau, C. & Sreenivasan, K. R. 1991 The multifractal nature of turbulent energy dissipation. *J. Fluid Mech.* **224**, 429–484.

Mydlarski, L. & Warhaft, Z. 1996 On the onset of high Reynolds number grid-generated wind-tunnel turbulence. *J. Fluid Mech.* **320**, 331–368.

Mydlarski, L. & Warhaft, Z. 1998 Passive scalar statistics in high-Péclet-number grid turbulence. *J. Fluid Mech.* **358**, 135–175.

Nelkin, N. & Chen, S. 1998 The scaling of pressure in isotropic turbulence. *Phys. Fluids* **10**, 2119–2121.

Obukhov, A. M. 1949 Pressure fluctuations in turbulent flow. *Dokl. Acad. Nauk. SSSR* **66**, 17–20.

Obukhov, A. M. & Yaglom, A. M. 1951 The microstructure of turbulent flow. *Prikl. Mat. Meckh.* **15**, 3–26 (Translation in *NACA TM* 1350, National Advisory Committee for Aeronautics, Washington, DC, June 1953.)

Pearson, B. R. & Antonia, R. A. 2001 Reynolds-number dependence of turbulent velocity and pressure increments. *J. Fluid Mech.* **444**, 343–382.

Pearson, B. R. & Krogstad, P. A. 2001 Further evidence for a transition in small-scale turbulence. In *Proc. 14th Australian Fluid Mechanics Conference, Adelaide, Australia* (ed. B. B. Daily), pp. 773–776. Adelaide University.

Pearson, B. R. Krogstad, P. A. & van de Water, W. 2000 The effect of large-scale forcing on the small-scale structure of turbulence. *Phys. Rev.* E (submitted).

Pumir, A. & Shraiman, B. I. 1995 Persistent small scale anisotropy in homogeneous shear flows. *Phys. Rev. Lett.* **75**, 3114–3117.

Shaw, R. A. 2003 Particle–turbulence interaction in clouds. *Annu. Rev. Fluid Mech.* **35**, 183–227.

Shen, X. & Warhaft, Z. 2000 The anisotropy of the small scale structure in high Reynolds number ($R_\lambda \sim 1000$) turbulent shear flow. *Phys. Fluids* **12**, 2976–2989.

Shen, X. & Warhaft, Z. 2002 Longitudinal and transverse structure functions in sheared and unsheared wind-tunnel turbulence. *Phys. Fluids* **14**, 370–381.

Sirivat, A. & Warhaft, Z. 1983 The effect of a passive cross-stream temperature gradient on the evolution of temperature variance and heat flux in grid turbulence. *J. Fluid Mech.* **128**, 323–346.

Sreenivasan, K. R. & Antonia, R. A. 1997 The phenomenology of small-scale turbulence. *Annu. Rev. Fluid Mech.* **29**, 435–472.

Tabeling, P. & Willaime, H. 2002 Transition at dissipative scales in large Reynolds number turbulence. *Phys. Rev.* E **65**, 066301–5.

Tabeling, P., Zocchi, G., Belin, F., Maurer, J. & Willaime, H. 1996 Probability density functions, skewness, and flatness in large Reynolds number turbulence. *Phys. Rev.* E **53**, 1613–1621.

Tsinober, A. 2001 *An Informal Introduction to Turbulence*. Kluwer.

Vedula, P. & Yeung, P. K. 1999 Similarity scaling of acceleration and pressure statistics in numerical simulations of isotropic turbulence. *Phys. Fluids* **11**, 1208–1220.

Voth, G. A., La Porta, A., Crawford, A. M., Alexander, J. & Bodenschatz, E. 2002 Measurements of particle accelerations in fully developed turbulence. *J. Fluid Mech.* **469**, 121–160.

Voth, G. A., Satyanarayan, K. & Bodenschatz, E. 1998 Lagrangian acceleration measurements at large Reynolds numbers. *Phys. Fluids* **10**, 2268–2280.

Warhaft, Z. 2000 Passive scalars in turbulent flows. *Annu. Rev. Fluid Mech.* **32**, 203–240.

Warhaft, Z. & Shen, X. 2002 On the higher order mixed structure functions in laboratory shear flow. *Phys. Fluids* **14**, 2432–2438.

Yaglom, A. M. 1949 On the field of accelerations in turbulent flow. *Dokl. Akad. Nauk. SSSR* **67**, 795–798.

Yoon, K. & Warhaft, Z. 1990 The evolution of grid generated turbulence under conditions of stable thermal stratification. *J. Fluid Mech.* **215**, 601–638.